AD-A048 157 BATTELLE COLUMBUS LABS OHIO F/G 4/2
METEOROLOGICAL SATELLITE OBSERVATIONS AND ARMY OPERATIONS.(U)
JUL 77 T T FUJITA DAAG29-76-D-0100
UNCLASSIFIED ECOM-77-6 NL

1 OF 1
ADA048 157

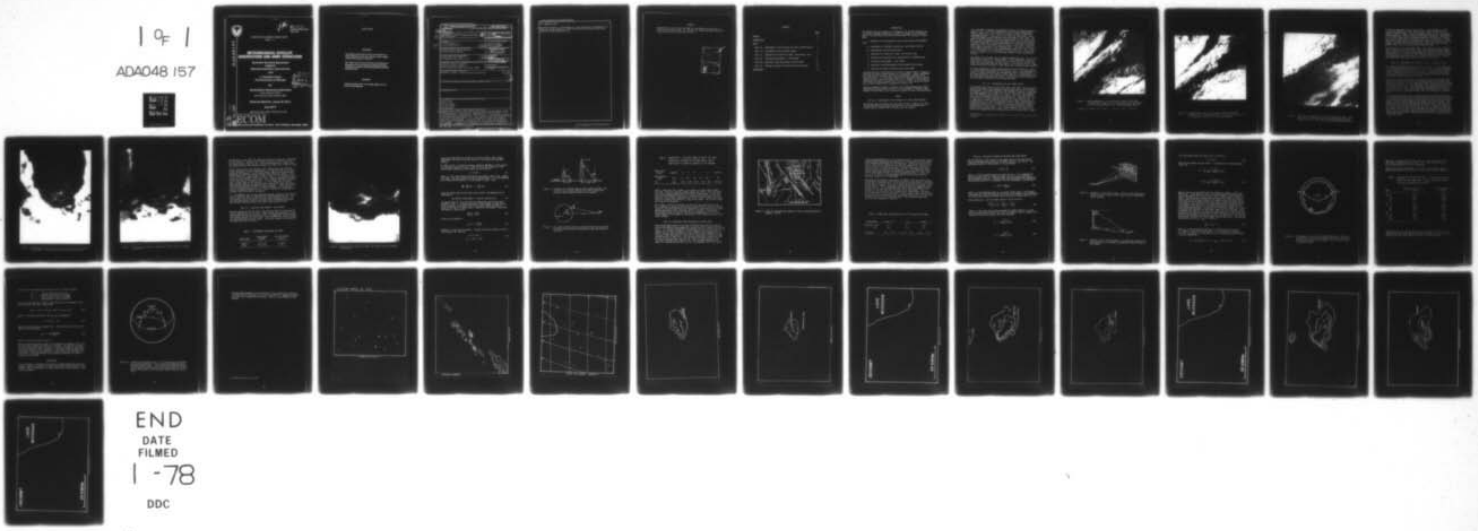

END
DATE FILMED
1-78
DDC

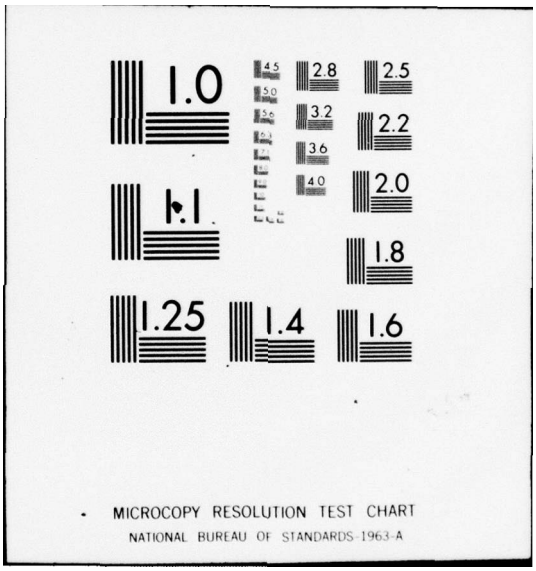
1.0
1.1
1.25
1.4
1.6
1.8
2.0
2.2
2.5
2.8
3.2
3.6
4.0
4.5
5.0
5.6
6.3
7.1
8.0
9.0
MICROCOPY RESOLUTION TEST CHART
NATIONAL BUREAU OF STANDARDS-1963-A

RESEARCH AND DEVELOPMENT TECHNICAL REPORT
ECOM - 77- 6

METEOROLOGICAL SATELLITE OBSERVATIONS AND ARMY OPERATIONS

Scientific Services Agreement
between
Battelle Columbus Laboratories
and

T. Theodore Fujita
The University of Chicago

for

Atmospheric Sciences Laboratory
US Army Electronics Command
White Sands Missile Range, New Mexico 88002

Contract Monitor: James D. Horn

July 1977

Approved for public release; distribution unlimited.

ECOM
UNITED STATES ARMY ELECTRONICS COMMAND - FORT MONMOUTH, NEW JERSEY 07703

NOTICES

Disclaimers

The findings in this report are not to be construed as an official Department of the Army position, unless so designated by other authorized documents.

The citation of trade names and names of manufacturers in this report is not to be construed as official Government indorsement or approval of commercial products or services referenced herein.

Disposition

Destroy this report when it is no longer needed. Do not return it to the originator.

SECURITY CLASSIFICATION OF THIS PAGE *(When Data Entered)*

REPORT DOCUMENTATION PAGE

READ INSTRUCTIONS BEFORE COMPLETING FORM

1. REPORT NUMBER: ECOM-77-6	2. GOVT ACCESSION NO.
3. RECIPIENT'S CATALOG NUMBER	
4. TITLE *(and Subtitle)*: METEOROLOGICAL SATELLITE OBSERVATIONS AND ARMY OPERATIONS.	5. TYPE OF REPORT & PERIOD COVERED: Final Report, 27 Oct 76 - 31 Mar 77
6. PERFORMING ORG. REPORT NUMBER	
7. AUTHOR(s): T. Theodore Fujita	8. CONTRACT OR GRANT NUMBER(s): DAAG29-76-D-0100
9. PERFORMING ORGANIZATION NAME AND ADDRESS: Battelle Columbus Laboratories and The University of Chicago	10. PROGRAM ELEMENT, PROJECT, TASK AREA & WORK UNIT NUMBERS: DA Task 1T162111AH71
11. CONTROLLING OFFICE NAME AND ADDRESS: US Army Electronics Command, Fort Monmouth, New Jersey 07703	12. REPORT DATE: July 1977
	13. NUMBER OF PAGES: 29
14. MONITORING AGENCY NAME & ADDRESS *(if different from Controlling Office)*: Atmospheric Sciences Laboratory, US Army Electronics Command, White Sands Missile Range, New Mexico 88002	15. SECURITY CLASS. (of this report): UNCLASSIFIED
	15a. DECLASSIFICATION/DOWNGRADING SCHEDULE

16. DISTRIBUTION STATEMENT *(of this Report)*
Approved for public release; distribution unlimited.

17. DISTRIBUTION STATEMENT *(of the abstract entered in Block 20, if different from Report)*

18. SUPPLEMENTARY NOTES

19. KEY WORDS *(Continue on reverse side if necessary and identify by block number)*
Severe storms
Rainfall rates
Satellite imagery
Cloud photography
Army operations

20. ABSTRACT *(Continue on reverse side if necessary and identify by block number)*
Determination of rainfall from satellite data requires the examination of the following features: (1) Watch for a rapid growth of the anvil cloud. It is a clear indication of strong updrafts inside the cloud. (2) Determine the motion of the head area on the upwind side. If the upwind side does not drift fast, or even stays at the same spot, it is an indication of a giant storm standing against the steering winds. (3) Rainfall does not end when the overshooting tops disappear. A ground truth experiment for interpretation of SMS/GOES data is presented. Included are: (1) techniques for cloud growth analyses from

DD FORM 1 JAN 73 1473 EDITION OF 1 NOV 65 IS OBSOLETE

SECURITY CLASSIFICATION OF THIS PAGE *(When Data Entered)*

20. ABSTRACT (cont)

successive pictures, (2) development of a time lapse whole sky photograph program, and (3) the solution of camera calibrations that relate to the cloud height and growth computations.

PREFACE

Appreciation is due to NESS and NOAA for the SMS/GOES pictures and to Illinois State Water Survey for supplying the author with excellent rain gauge data covering Chicago and vicinity.

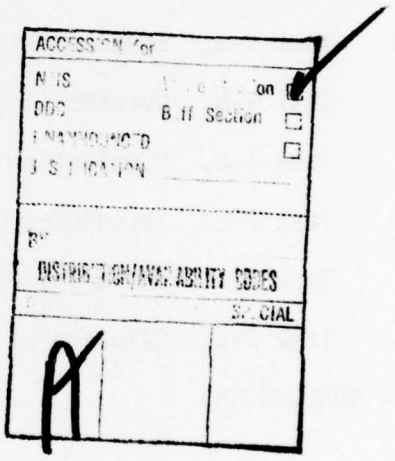

CONTENTS

INTRODUCTION

The objective of this report is to interpret, for US Army mesoscale applications, SMS/GOES meteorological satellite imagery by all feasible means. The following tasks were performed under the contractual agreement:

1. Analyses of three mesoscale severe storm cases using SMS/GOES data

   a. Enhancement of SMS/GOES pictures for storm identification

   b. Overshooting tops and radar echoes

   c. Combination of satellite, radar, and rainfall data

2. Ground-truth experiment for interpretation of SMS/GOES data

   a. Techniques development: cloud growth

   b. Whole-sky cloud photography at White Sands Missile Range

   c. Solution of camera calibration and cloud height

The availability of high-resolution satellite imagery offers a unique opportunity to monitor severe weather on the mesoscale. Often, meteorological data are not available for tactical operations, especially over enemy territory. It is extremely important to determine areas of severe convective activities which might give rise to changes in trafficability. Trafficability could be reduced to a difficult or even impossible degree due to severe thunderstorms accompanied by heavy rain.

Since no convective clouds of interest to the Army developed over White Sands Missile Range during the life of this agreement (27 October 1976 through 31 March 1977), only theoretical aspects of task 2 were performed.

TASKS

Task 1-a. Enhancement of SMS Pictures for Storm Identification

During past years the author has assisted the Army in making film loops for the purpose of computing cloud motions. For this purpose small clouds, such as cumulus and/or stratus, must be tracked.

It is desirable to enhance low-brightness clouds for tracking purposes. Shown in Figs. 1 and 2* are examples of light and dark enhancements. Cumulus clouds (M, N, O) in Fig. 1 are clearly visible in the light-enhancement picture. Thin cirrus (P, Q) are also significant in the light-enhancement picture because their background is dark ocean. The mouth of the Mississippi River also appears better in the light print. Most storms are embedded inside the bright anvil clouds often produced by storms themselves. Without enhancement the storm areas are usually washed out into a large white mass of clouds. A very small cloud (A) can be seen in either picture reasonably well. The tops of storms B, C, D are identifiable only in the dark-enhanced picture (Fig. 2). Storms F, G, H are brought out significantly in the dark print. Similar features of clouds I, J, K, L are also seen clearly in the dark-enhanced picture.

The reason for the bright tops of growing thunderstorm are: (1) an overshooting top consists of a large number of small hydrometeors which reflect light significantly, (2) the top is so high that it is under the bright sun, way above haze and dust layers, (3) a slanted side of a huge cloud top receives sunlight at right angle, thus reflecting more sunlight.

A proper enhancement, either photographically or electronically results in a significant improvement of the cloud top image. Dark enhancement is useful in showing distinctly the overshooting tops of thunderstorms. It was found during the last couple of years that not all overshooting tops are associated with severe activities. Furthermore, severe activities are not always characterized by overshooting tops.

Task 1-b. Overshooting Tops and Radar Echoes

An overshooting at the anvil-top level takes place when a fast-rising air keeps rising against the negatively buoyant lapse rate at the lowermost stratosphere. The updraft speeds in the thunderstorm may be so high that the upward momentum will propel the cloud air much above the tropopause until the downward force brings it to a halt. Both rain and downdraft occur where the downward currents are predominant. Therefore, the area of heavy rain is often displaced from that of an overshooting top. It is necessary to combine satellite pictures with radar pictures with an extreme accuracy, in order to determine rainfall versus overshooting relationship (see Fig. 3). The areas A B are characterized by a rather bright deck of cirrus cloud. It is an old squall line which could redevelop into an active squall line. Cloud C denotes the location of a radar echo accompanied by an overshooting top on its west side. Cloud D

Overlays for all figures are included in the envelope in the back of this document.

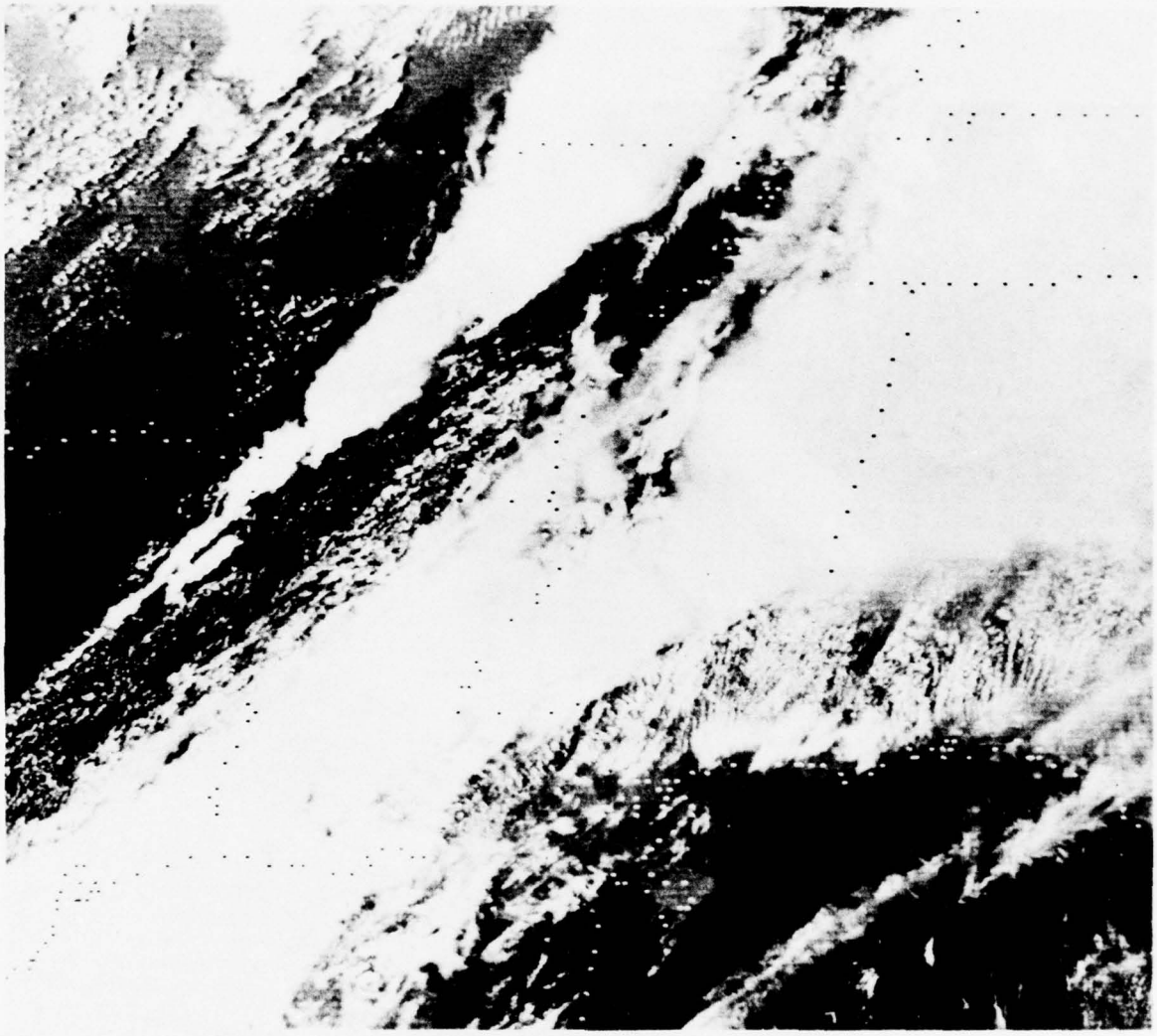

Figure 1. Light enhancement of an SMS picture started at 2132 GMT, 29 March 1976. Cumuli, M, N, O* and faint cirrus over water, P, Q,* are well-defined in this light-enhancement picture.

*Overlays to figures are included in envelope in back of document.

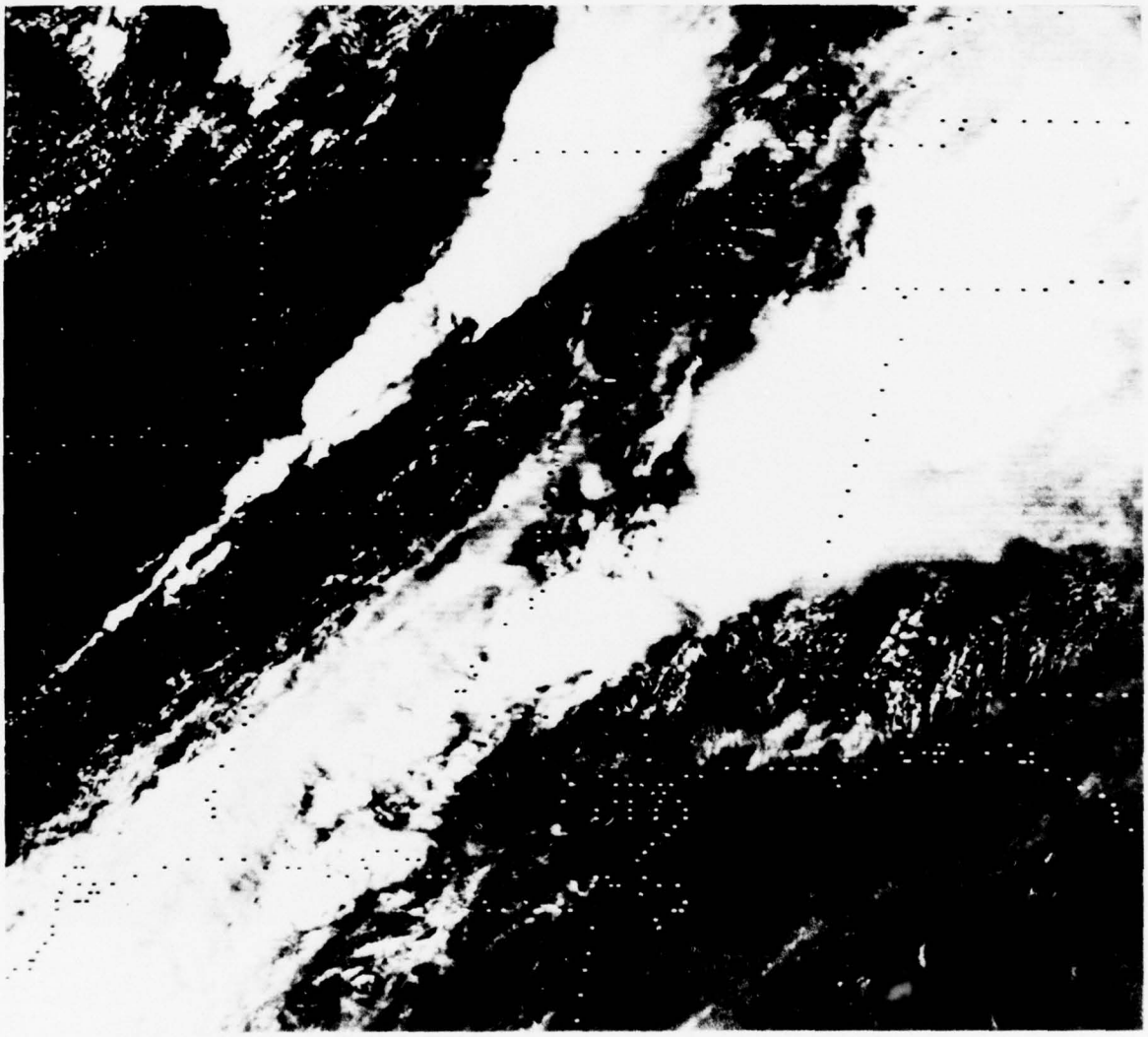

Figure 2. Dark enhancement of an SMS picture started at 2132 GMT, 29 March 1976. Huge thunderstorms, B, C, D, F, G, H, I, J, K, L, are now seen against their cirrus environment.

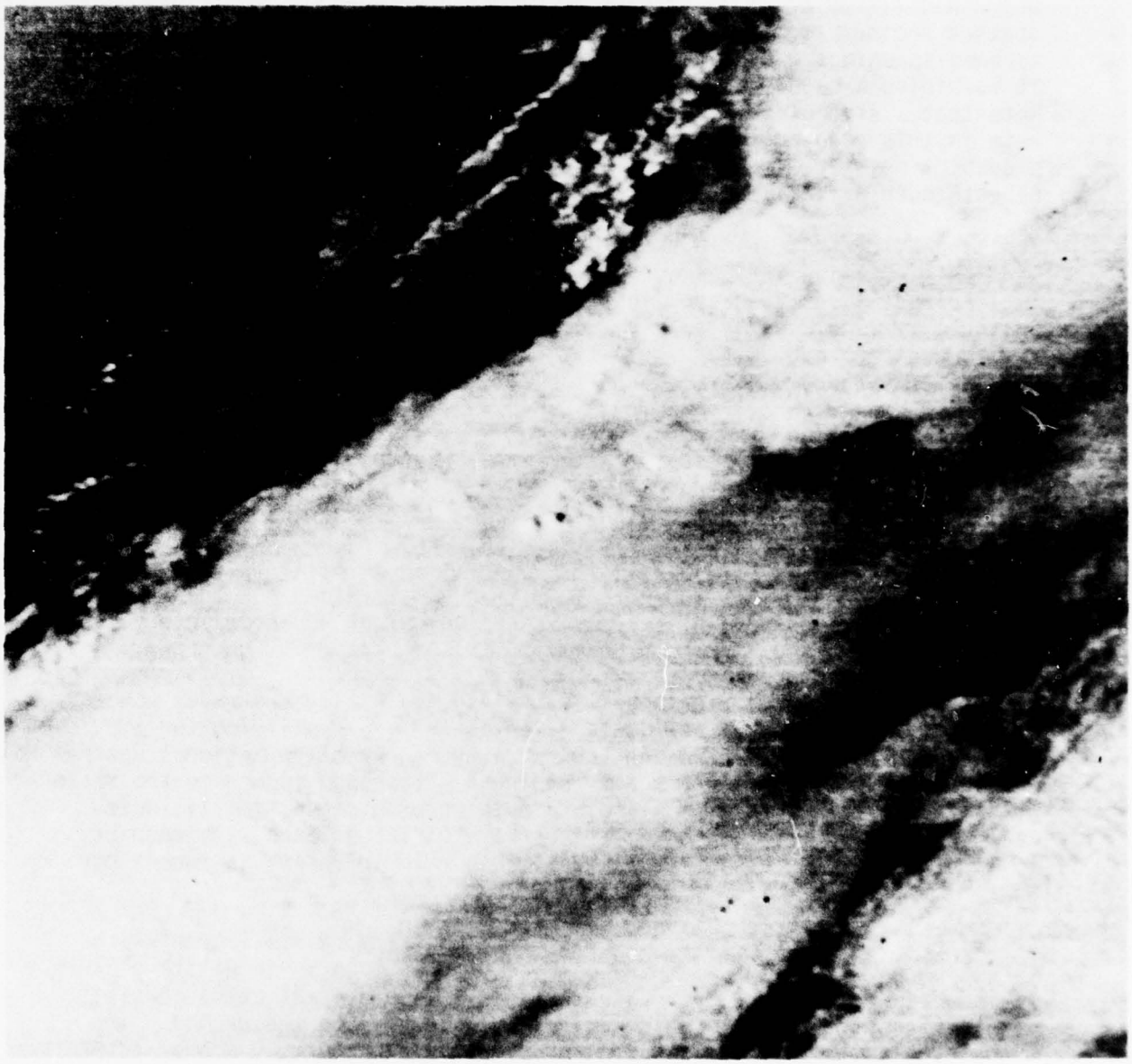

Figure 3. Relationship between radar echo and overshooting areas. Note that not all overshooting areas are characterized by radar echoes and not all radar echo areas show overshooting features.

is the most dangerous cloud in the picture. It had spawned a tornado which had lifted prior to this picture time. About 25 min later it spawned another tornado. Such an overshooting top is often seen between tornado spawnings. Cloud E has no overshooting whatsoever. Nonetheless, it is hiding a huge mass of raindrops beneath an extensive anvil cloud. Note that a strong echo is seen where the letter E is located. Rainfall rate in this echo could be as much as one to two inches per hour. At the present time there is no way of detecting a high-liquid-water content beneath such a flat cirrus cloud using satellite data.

The line F, G, H is an old squall line. Just like line AB this squall line reintensified into an active squall line, spawning several tornadoes. Small clouds I, J, K, L are lines of cumuli on the dry-air side of the instability line. A large area indicated by M and N are high thin clouds from downstream convective activity. Usually these clouds are so thin that underlying cumuliform clouds could be seen if present.

Task 1-c. Combination of Satellite, Radar, and Rainfall Data

It is rather difficult to combine satellite and radar pictures with rainfall data, because mesoscale rain gauge networks do not exist everywhere. A rare comparison was made possible by the Illinois State Water Survey's network around the south end of Lake Michigan. Obtained for this task are three situations of severe storms development at one-hour intervals, 2200, 2300, and 2400 GMT on 13 June 1976.

Figure 4 is a color combination of satellite, rainfall, and radar echoes. The satellite picture was produced by enlarging and rectifying the SMS picture for 2200 GMT. Echo contours were traced from the National Weather Service, Marseilles radar after enlarging a PPI scope picture to the scale of the satellite picture. Rain gauge data were obtained from Illinois State Water Survey. Rain gauge traces were differentiated with respect to time to convert cumulative rainfall into rain intensity in inches per hour.

A striking result seen in Fig. 4 is the size of the rainfall area which is considerably smaller than the outline of the cloud in satellite picture. It is because the cloud area, as storm grows into a giant cell, consists mainly of anvil materials which do not produce rain on the ground. The highest rainfall rate at 2200 GMT was 0.8 inch per hour. One hour later, at 2300 GMT, the rainstorm intensified, producing a rate of 3.3 inches per hour at one point in the city (see Fig. 5). It should be noted that the rainfall cell is small and located near the west edge of a huge anvil cloud. At this time radar detected a small echo inside a cloud near the north edge of the picture. The rainfall rate from this cloud was significant at this time.

Figure 4. Combination of satellite, radar, and rainfall data at 2200 GMT, 13 June 1976. A flash flood case in Chicago and vicinity.

Figure 5. Combination of satellite, radar, and rainfall data at 2300 GMT, 13 June 1976.

By 2400 GMT, 13 June 1976, the rainstorm grew into a giant cell with radar echo at level 4+. Surface rainfall was in excess of 3 inches per hour at several centers (see Fig. 6). The Dan Ryan Expressway, a major highway extending south from downtown Chicago, was under 3 to 10 feet of water.

If this kind of heavy rain persists over a combat area, the field will become impassable. Proper interpretation of satellite data is the key to prediction and warning. The following points should be considered when attempting to determine rainfall amounts from convective clouds. First of all "watch for a rapid growth of anvil cloud." It is the clear indication of strong updrafts inside the cloud. Second, "determine the motion of the head area on the upwind side." If the upwind side does not drift fast, or even stays at the same spot, it is an indication of a giant storm standing against the steering winds. And third, "note that rainstorm does not end when overshooting tops disappear." After the dissipation of overshooting activities, a significant amount of liquid water could be suspended beneath the anvil cloud. The end of overshooting by no means signals the end of rainstorms.

It is recommended that the Army undertake further research on the application of satellite data to trafficability forecasting and warning. For this purpose, the ground station at White Sands should be used in full. The Army should obtain digital and visual data of SMS/GOES, especially the 3-minute rapid scan data to be taken in the spring of 1977.

Task 2-a. Techniques Development: Cloud Growth

When one watches an SMS film loop, there are two types of cloud motions clearly identifiable on the image. These motions are related to (1) the displacement and (2) the vertical growth. The magnitude of the displacement varies according to cloud types. Their extremes are found in tracking cumuliform and cirriform clouds. The typical ranges of displacement and growth are found in Table 1.

TABLE 1. DISPLACEMENT AND GROWTH OF CLOUDS

Cloud Types	Displacement (m/sec)	Vertical Growth (m/sec)
Cumulus	5 to 20	2 to 10
Cirrus	30 to 100	0 to 1

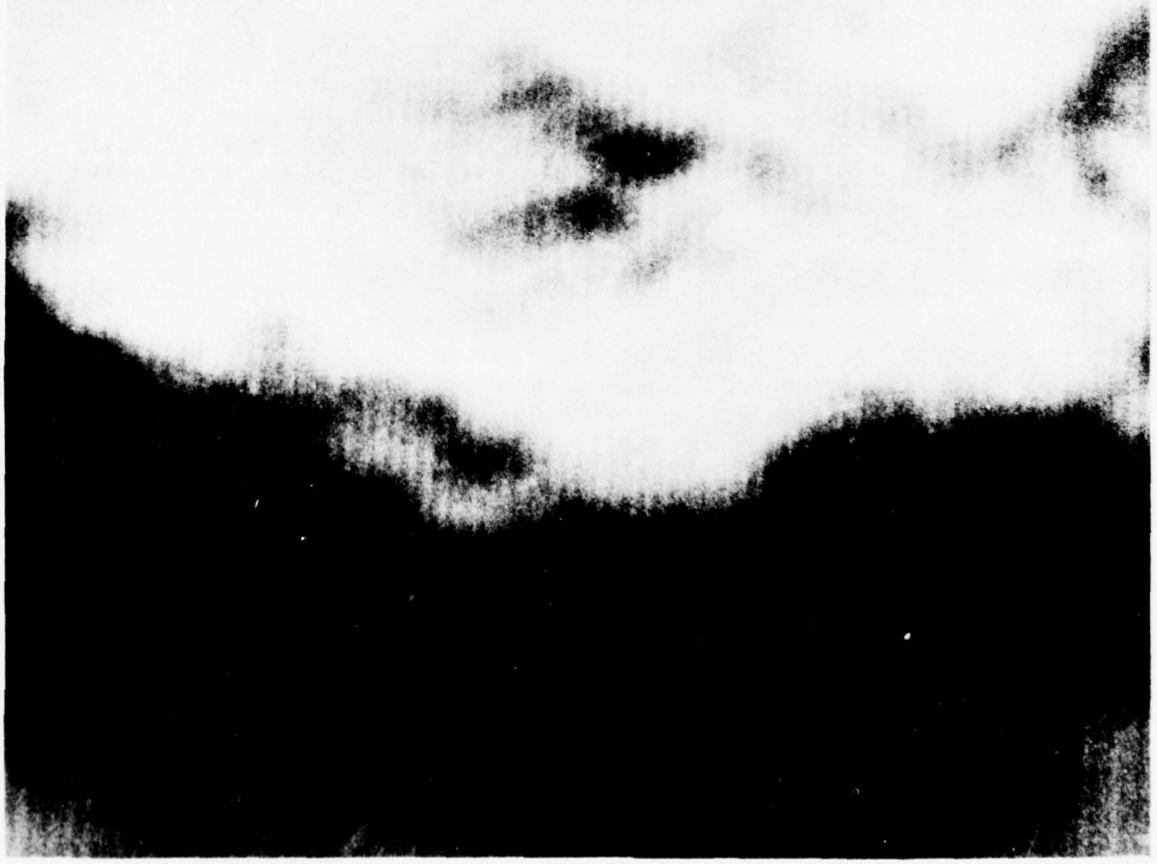

Figure 6. Combination of satellite, radar, and rainfall data at 2400 GMT, 13 June 1976.

Since the growth rates of clouds are closely related to their future development, we have to know the effects of the growth upon SMS/GOES imagery.

As shown in Fig. 7, clouds are always viewed by SMS/GOES in slant angles. Let the zenith angle of view be ζ and the cloud top height be H; the cloud height projected on the surface can be written as

$$X = H \tan \zeta \tag{1}$$

where X is the cloud height projected on the ground. Both H and ζ change with time. The time variation of the projected height, X, can be obtained by differentiating Equation (1) with respect to time. Thus,

$$\frac{dx}{dt} = \frac{dh}{dt} \tan \zeta + H \frac{d\zeta}{dt} \sec^2 \zeta \tag{2}$$

Since the second term on the right side is small, the equation can be rewritten as

$$\text{horizontal displacement} = (\text{vertical growth}) \tan \zeta \tag{3}$$

The zenith angle of view can easily be obtained by solving the plane triangle in Fig. 8. β denotes geocentric angle between a cloud and satellite subpoint, γ the nadir angle of the cloud viewed from SMS, R $\simeq$ 6,380 km, the earth's radius, and D $\simeq$ 36,000 km, the height of SMS above the equator. Now we write

$$\frac{\sin \zeta}{R + D} = \frac{\sin \gamma}{R} \tag{4}$$

which can be reduced to

$$\sin \zeta = \gamma \frac{R + D}{R} \tag{5}$$

because γ is less than 10 degrees. Putting the actual values of R and D into Equation (5), we have

$$\sin \zeta = 6.6 \gamma \tag{6}$$

$$\text{or } \zeta = \sin^{-1} 6.6 \gamma$$

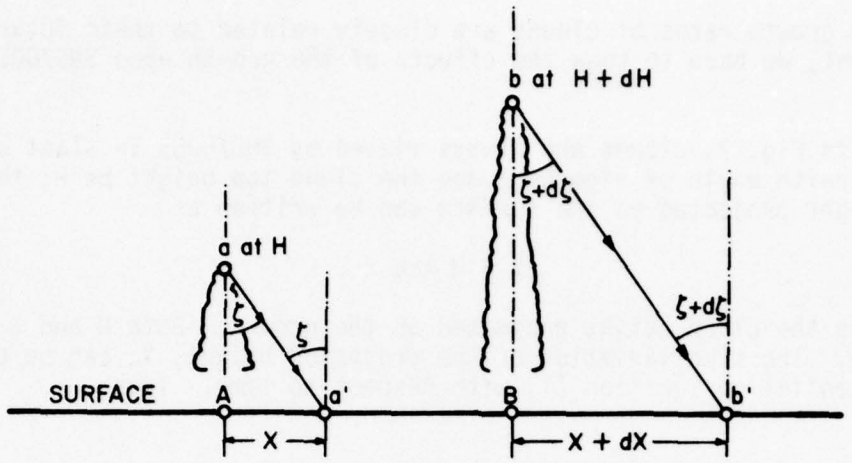

Figure 7. Schematic of a growing cumulus cloud viewed from SMS. Due to slant angle of view, SMS does not look straight down except at the subsatellite point on the equator.

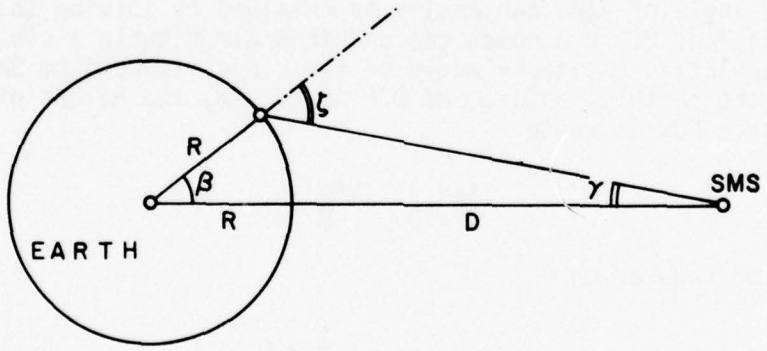

Figure 8. The zenith angle of view of a cloud from SMS can be obtained by solving the triangle including SMS, cloud, and center of the earth.

TABLE 2. VARIATION OF ζ, THE ZENITH ANGLE OF SMS AT THE CLOUD LOCATION AS A FUNCTION OF THE NADIR ANGLE γ WHICH VARIES FROM 1 TO ABOUT 8.6 DEGREES (AT THE HORIZON).

Nadir angle, γ(deg)	Subpoint	2	4	6	7	8	Horizon
Zenith angle, ζ(deg)	zero	13	28	44	54	68	90
Tan ζ	zero	0.23	0.53	0.96	1.38	2.48	infinity

Table 2 shows that tan ζ exceeds 1.0 at about a 6° nadir angle viewed from SMS. From that location outward toward the earth's limb, the effect of vertical growth exceeds that of horizontal displacement. This means that one could determine the vertical cloud growth by tracking the cloud motion on a loop image. Meanwhile, one cannot estimate cloud velocities simply by tracking the motions of cloud on the image. The vertical growth will have to be corrected.

White Sands, at 32.4° N latitude, can never be seen vertically by SMS. It is possible to determine the vertical growth rate of cumuliform clouds, especially the ones which grow over mountains, by examining carefully SMS imagery obtained at close intervals such as 3 minutes. The National Environmental Satellite Service (NESS) has announced that 11 days of 3-minute imagery will be taken in the Spring of 1977 beginning on storm days after 22 March.

Task 2-b. Whole-sky Cloud Photography at White Sands

Three-minute SMS pictures to be taken by NESS on storm days this spring will provide WSMR the best opportunity to perform their cloud-truth experiment. It is highly recommended that SMS/GOES data, for both IR and visible imagery, be recorded on tapes for future playback into pictorial and/or digital charts. Also two whole-sky cloud cameras are recommended for operation at WSMR beginning with the onset of the moisture inflow from the southeast early in June 1977. The Sacramento Mountains northeast of WSMR will be the best possible location for convective storms with a fixed location of updraft areas (see Fig. 9). The Sacramento Mountains are ideal for intercepting the moist air from the southeast with their gentle

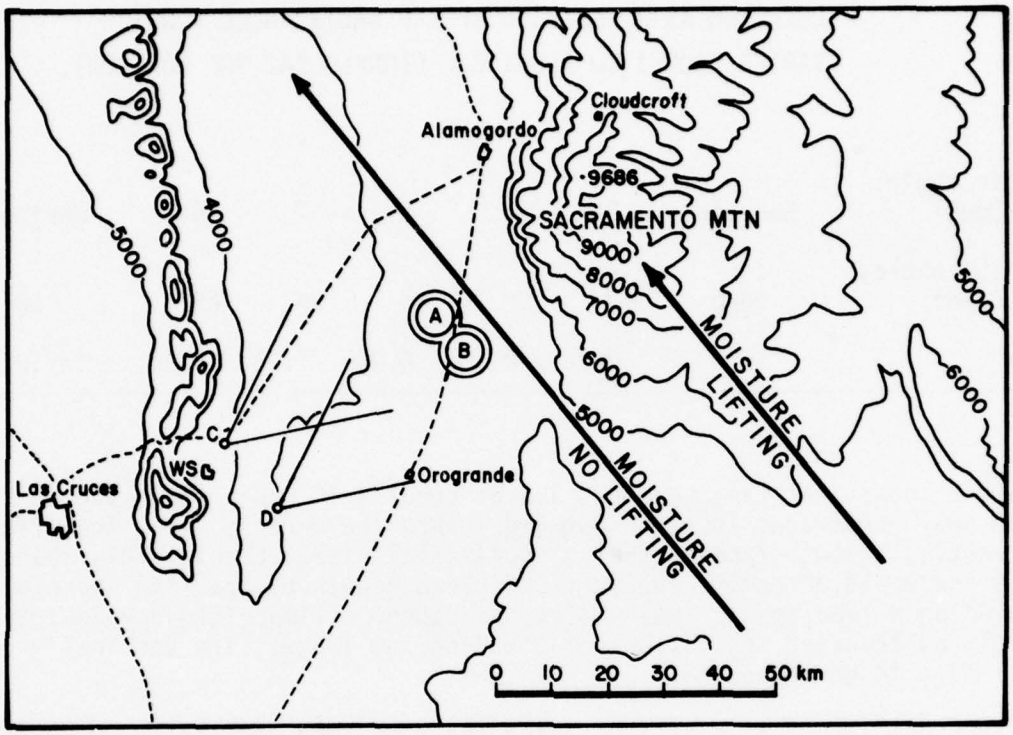

Figure 9. Sites for two whole-sky cameras, A and B, and two wide-angle cameras, C and D.

slope facing perpendicular to the inflow direction. Two whole-sky cameras placed between Alamogordo and Orogrande will be capable of recording the cloud formation and growth over the mountains. These cameras also will monitor the moisture inflow passing over the camera site. Since no lifting of moist air is expected to occur over the camera site, films will show the effect of both lifting and no lifting. Two wide-angle cameras looking toward the northeast from WSMR will record the side view of the entire neph-system forming over the Sacramento Mountains. A base line of 1.6 km (1 mile) for the wide-angle and 0.8 km (0.5 mile) for the whole-sky stereo pair is recommended.

According to the author's experience, the image of the sun moving across the whole-sky image does not interfere with the cloud analysis. The image of the sun is so small that it is no more than the size of a small cloud. No sun shade is needed. Wide-angle cameras should not be operated facing toward the sun. It is recommended that these cameras at WSMR be turned on after 10 a.m. MDT when the sun moves out of the camera's view. A 100-ft roll of 16-mm color film includes about 4000 frames. To assure no possible break of the scene within a day, a proper frame rate will have to be selected. As shown in Table 3 the frame rate of 5 to 7 sec will be the best in order not to break the scene in the afternoon hours when activities are expected to continue.

TABLE 3. FRAME RATES AND DURATION OF 100-FOOT COLOR FILM (16 MM).

Frame Rates	Every 5 sec	7 sec	10 sec
Durations (min)	333	467	667
(h)	5.6	7.8	11.1
Durations	1:30 - 7 p.m.	11 a.m. - 7 p.m.	8 a.m. - 7 p.m.

Task 2-c. Solution of Camera Calibration and Cloud Height

Let the effective focal length of the camera lens be f and the coordinates on the image relative to the principal point, P, be X and Y. The horizontal angle of a cloud point, C, can be written

$$\theta + \tan^{-1} \frac{X}{f} \tag{7}$$

where θ is the horizontal angle of C (see Fig. 10). It is important to keep the optical axis of the movie-camera lens as close as possible to the horizontal direction. Otherwise the solution becomes more complicated. The elevation angle of C is computed from the trigonometric relationship,

$$\phi = \tan^{-1} \frac{Y}{f \sec \phi} \tag{8}$$

where ϕ is the elevation angle of C, a point on the cloud. The distance from camera to cloud which may be called the cloud distance can be computed by solving the triangle including the cloud and two cameras (see Fig. 11).

After obtaining θ, the horizontal angle of cloud, we write

$$\frac{\sin(\theta_1 - \theta_2)}{L} = \frac{\cos \theta_1}{D_2} = \frac{\cos \theta_2}{D_1} \tag{9}$$

where L is the base-line distance between two stereo cameras, D is the cloud distance, and suffixes 1 and 2 are for cameras C and D, respectively. From this solution we express the cloud distances:

$$D_1 = L \frac{\cos \theta_2}{\sin(\theta_1 - \theta_2)} \tag{10}$$

$$D_2 = L \frac{\cos \theta_1}{\sin(\theta_1 - \theta_2)} \tag{11}$$

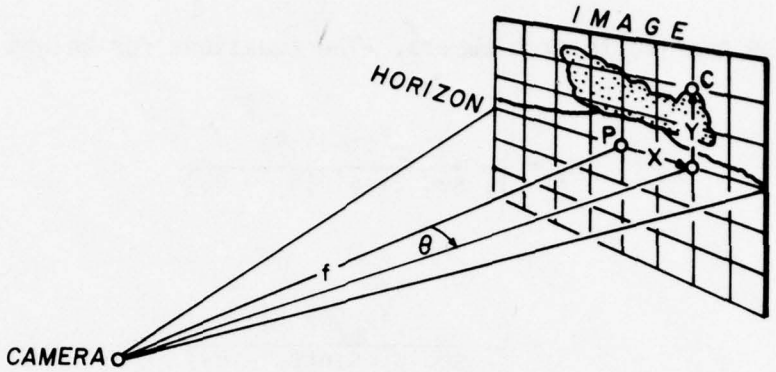

Figure 10. Geometry of a horizontal image. No tilt of the camera axis should be used in order to avoid complication of photogrammetric analyses.

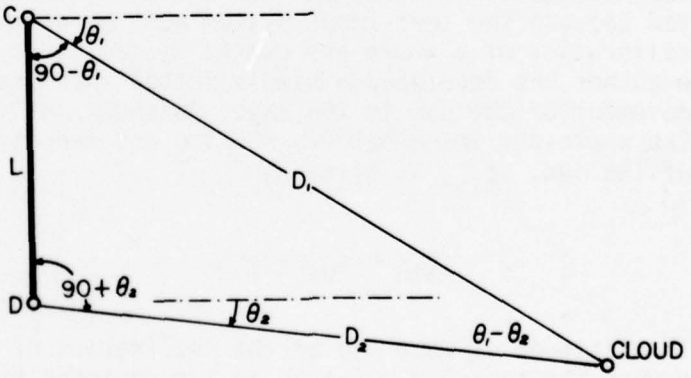

Figure 11. Solution of the cloud distance, D. A stereo pair permits the cloud distance to be computed independently from the image of each camera.

The cloud height above the camera site is written as

$$H = D \tan \phi \tag{12}$$

which can be applied to each camera. The equations for height computations are:

$$H_1 = \frac{L}{f_1} \frac{Y_1 \cos \theta_2}{\sec \theta_1 \sin(\theta_1 - \theta_2)}$$

$$H_2 = \frac{L}{f_2} \frac{Y_2 \cos \theta_1}{\sec \theta_2 \sin(\theta_1 - \theta_2)} \tag{13}$$

Where f_1 and f_2 are the effective focal lengths of cameras C and D, respectively. These equations indicate that the images from each camera can be enlarged to any size as long as their effective focal lengths are known. The elevation of cameras does not have to be identical, because the computed cloud height represents the height above the camera elevation which should be added to the cloud height in order to obtain the MSL cloud height. The solution of the stereo measurements presented herein is extremely simple and useful in determining kinematic properties of cloud growth and movement. A stereo pair of whole-sky cameras is slightly more complicated because the lens-image system must be calibrated. Since a laboratory calibration of a whole-sky camera system is complicated and expensive, the author has developed a simple method which can be performed by using the movement of the sun in the sky. As shown in Fig. 12, the sun moves across the whole-sky image between sunrise and sunset. The smallest zenith angle of the sun, ζ^*_{min}, is given by

$$\zeta^*_{min} = \phi_{ws} - \phi^* \tag{14}$$

where ϕ_{ws} is the latitude of WSMR and ϕ^* the declination of the sun. ϕ^* is positive when the subsolar point is in the northern hemisphere. The time, T_s, denotes the time when the sun is located due south of WSMR. It can be computed by

$$T_s = 12 \text{ h } 00 \text{ min} + \text{E.T.} + (\phi_{ws} - 105°) \times 4 \text{ min} \tag{15}$$

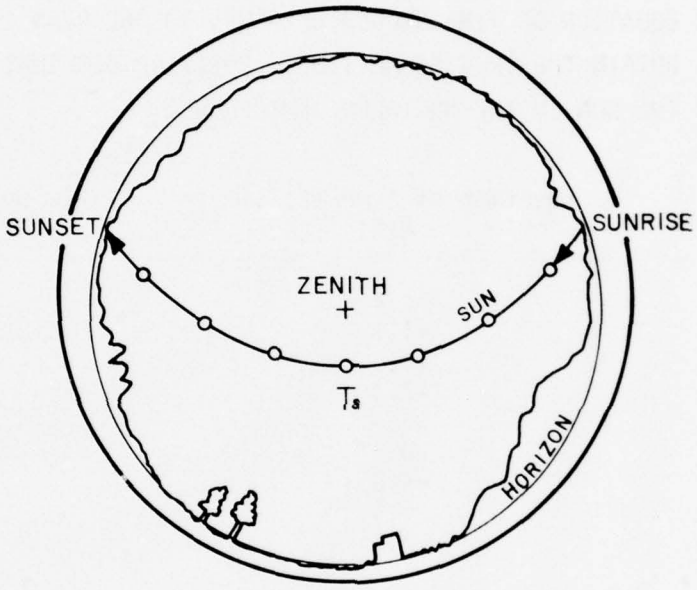

Figure 12. The movement of the sun on the whole-sky image. Since the positions of the sun can be computed easily as a function of time for any given day, the images of the sun serve as good calibration targets.

where E.T. is the equation of time which is to be added to mean solar time (MST) to obtain true solar time. (ϕ_{WS} - 105°) x 4 min is +6 min at White Sands and +4 min at Alamogordo.

Shown in Table 4 are the values of E.T. and ϕ^* during June - August period when convective activities are expected in the White Sands area.

TABLE 4. EQUATION OF TIME SHOULD BE ADDED TO THE MEAN SOLAR TIME TO OBTAIN THE TRUE SOLAR TIME. POSITIVE DECLINATION DENOTES THE SUN IN THE NORTHERN HEMISPHERES

Date	Equation of Time (E.T.) (min)	Declination (ϕ^*) (deg)
Jun 1	+2.4	+21.9
9	+1.1	+22.9
17	-0.5	+23.3
25	-2.3	+23.4
Jul 1	-3.5	+23.2
9	-4.9	+22.5
17	-5.9	+21.3
25	-6.4	+19.8
Aug 1	-6.3	+18.2
9	-5.6	+16.1
17	-4.2	+13.7
25	-2.3	+11.0

As shown in Fig. 12, the sun moves across the whole-sky image. If both zenith angle and azimuth angle of the sun are known as a function of time, images of the sun can be used as accurate calibration points.

Solutions can be obtained with the help of Fig. 13 which includes

θ^*. . . . . Relative longitude of the sun
α^*. . . . . Azimuth angle of the sun at WSMR
ζ^*. . . . . Zenith angle of the sun at WSMR
ϕ^*. . . . . Declination of the sun (Table 4)

By solving the spherical triangle, WSMR, North Pole, and Subsolar point, we first obtain the solar zenith angle.

$$\cos \zeta^* = \sin \phi^* \sin \phi_{ws} + \cos \phi^* \cos \phi_{ws} \cos \theta^* \tag{16}$$

where θ^*, relative longitude of the sun can be computed by

$$\theta^* = 15^\circ(Ts - Tm) \tag{17}$$

where Tm denotes Mountain Standard Time. The azimuth angle of the sun at WSMR can be calculated by

$$\sin \alpha^* = \frac{\cos \phi^* \sin \theta^*}{\sin \zeta^*} \tag{18}$$

where θ^* varies with time, so does ζ^*.

Now the azimuth and zenith angles can be computed by Equations (16), (17), and (18) and the whole-sky views are calibrated. The accuracy of these angles must be better than 0.5 degree. Finally any number of cloud points are to be selected to form stereo-pairs, and their horizontal angles are calculated. Using the same technique of determining cloud positions and height from a wide-angle stereo pair, kinematic parameters of growing clouds can be obtained.

CONCLUSIONS

Tasks a through c performed by the author for WSMR revealed the values of SMS/GOES imagery in relation to radar echoes and rainfall patterns on the ground. Their relationships are highly complicated, necessitating a cloud-truth experiment.

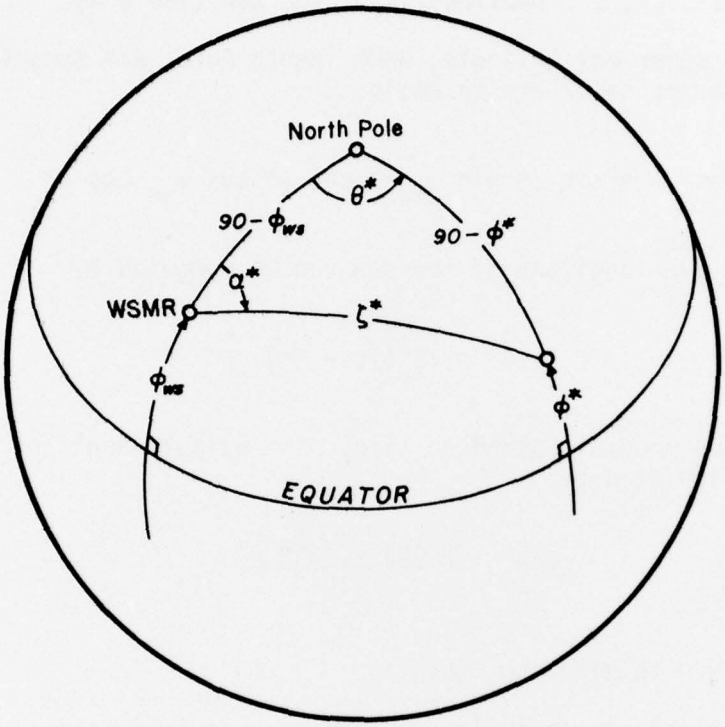

Figure 13. Azimuth (α^*) and zenith angle (ζ^*) of the sun can be computed by solving the spherical triangle connecting WSMR with North Pole and subsolar point. The accuracy of computations depends mainly upon the determination of both azimuth and zenith angle of each cloud point on the whole-sky images forming a stereo-pair.

The Sacramento Mountains to the northeast of White Sands will provide an excellent natural laboratory for cloud investigations. Methods of operating stereo-pair cameras were evaluated, leading to the solution of this problem.

☆U.S. GOVERNMENT PRINTING OFFICE: 1977 777-022/12

2132 GMT MARCH 29, 1976

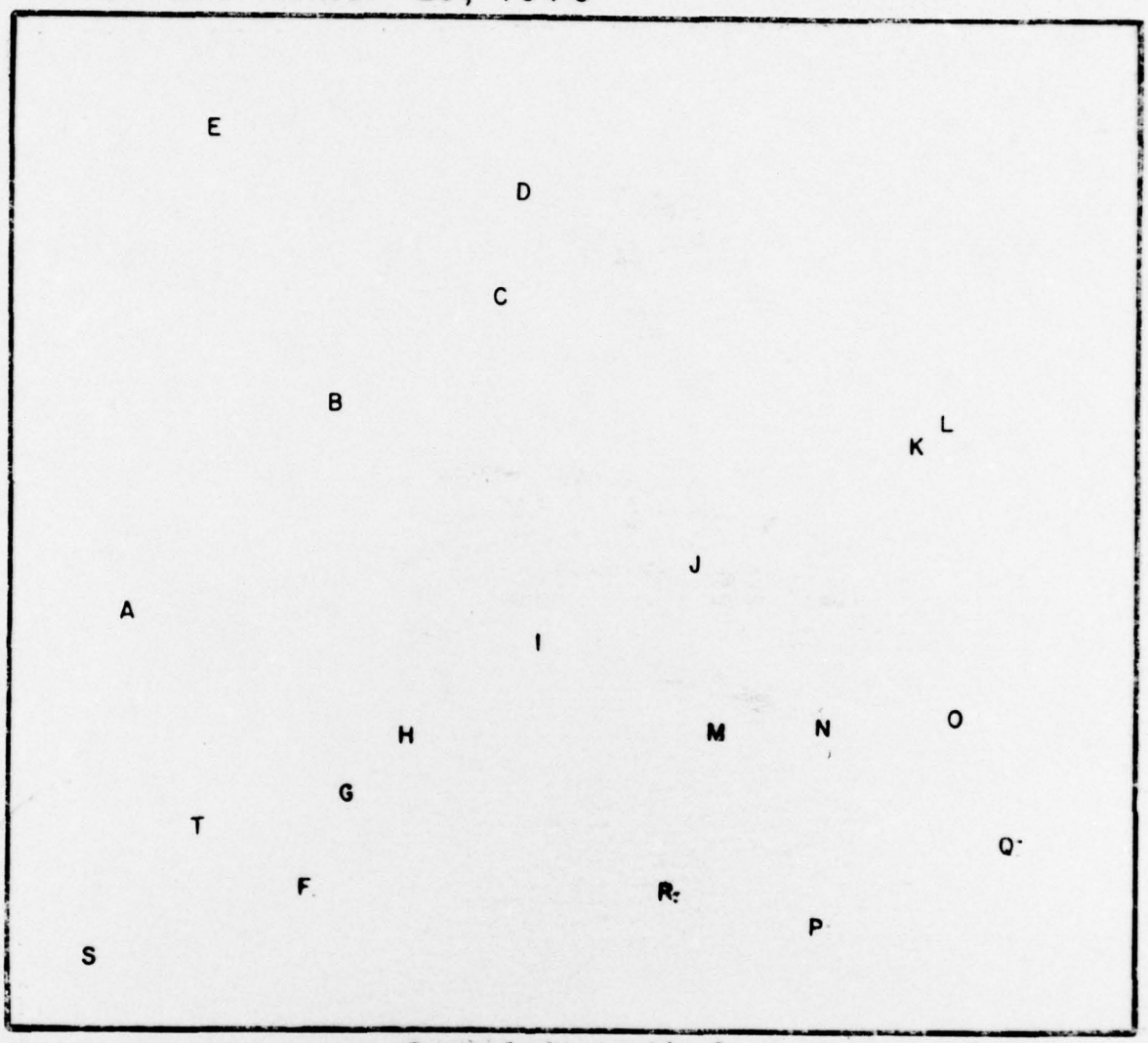

Overlay for fig. 1 and fig. 2

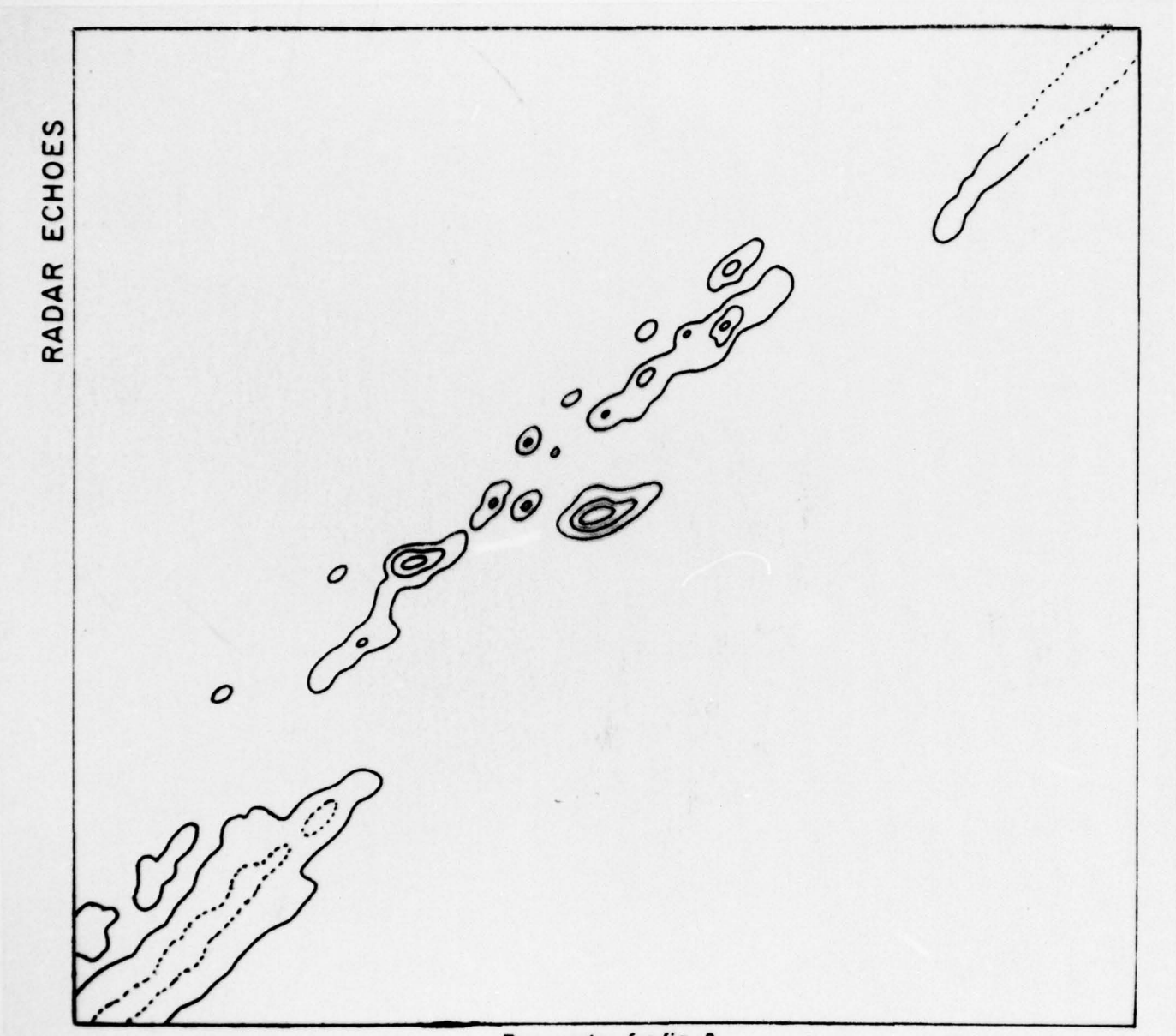

Top overlay for fig. 3

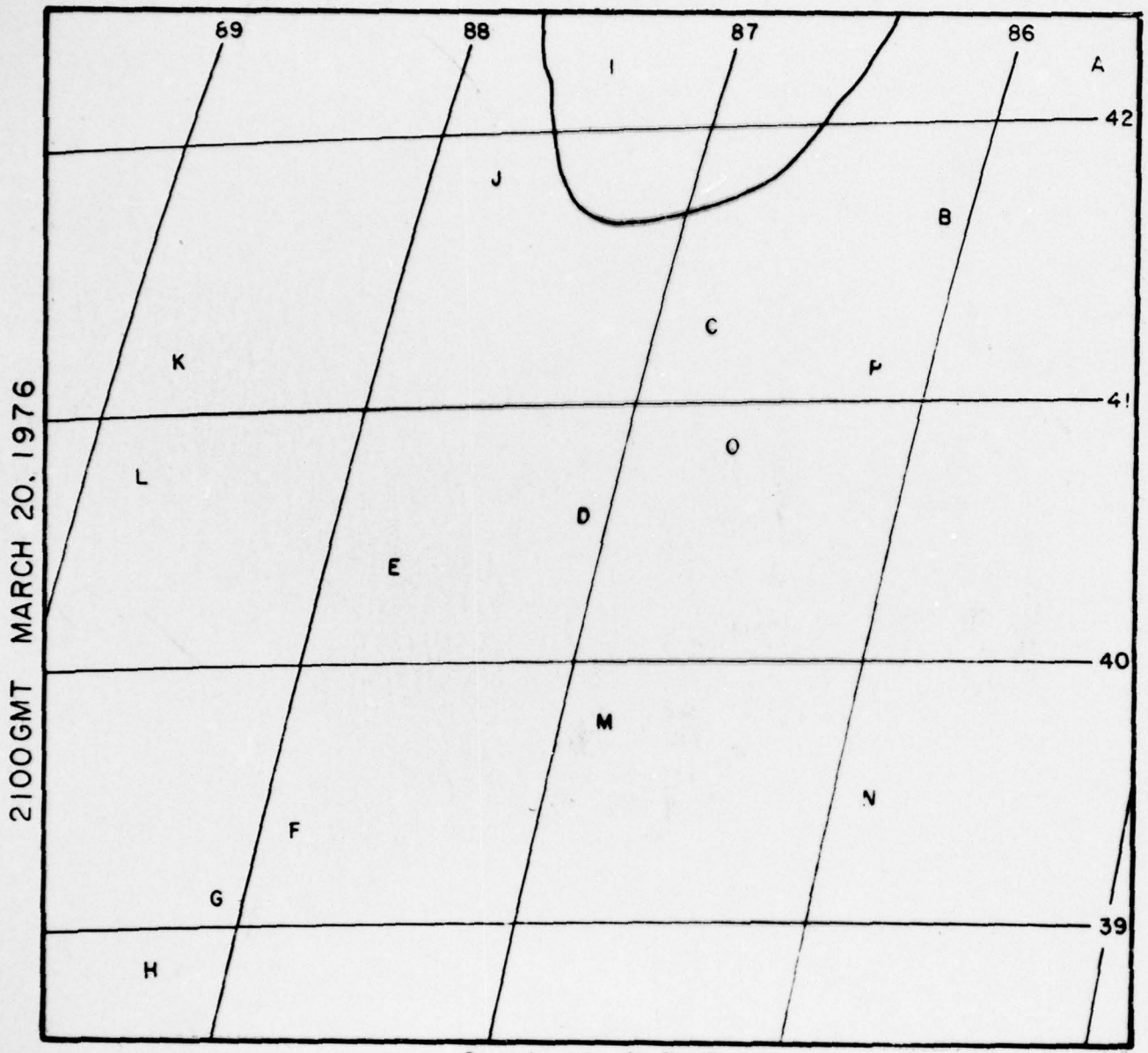

Second overlay for fig. 3

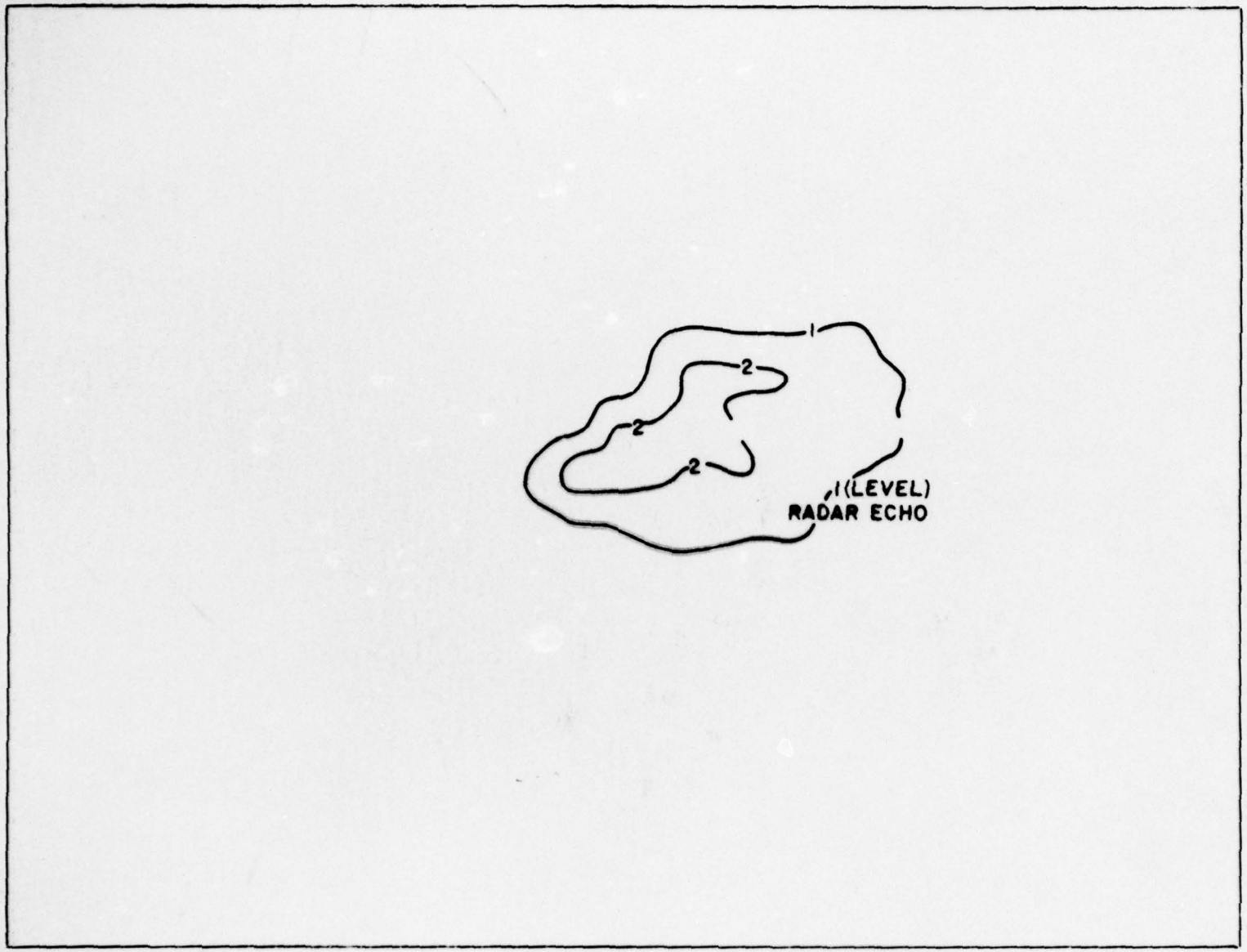

Top overlay for fig. 4

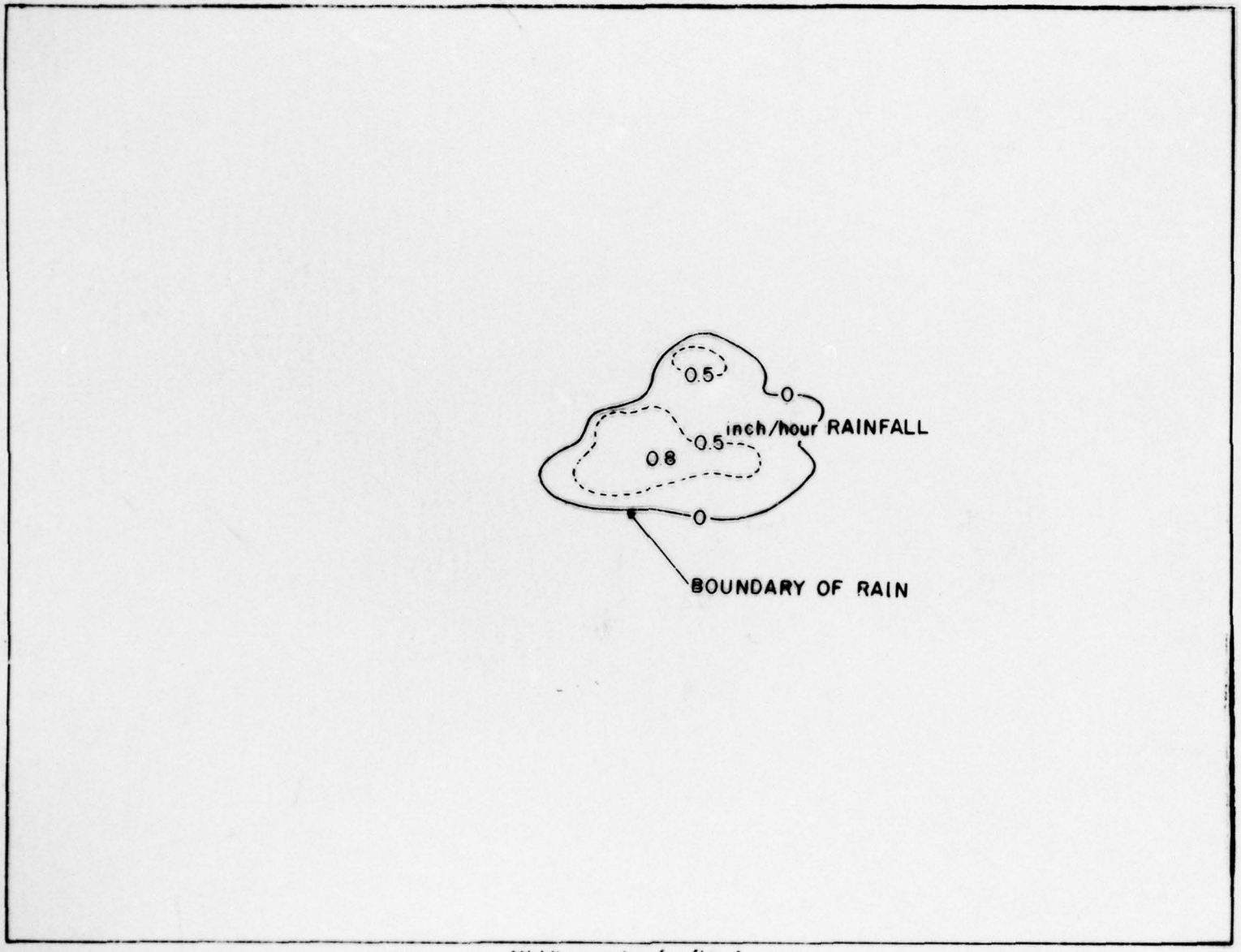

Middle overlay for fig. 4

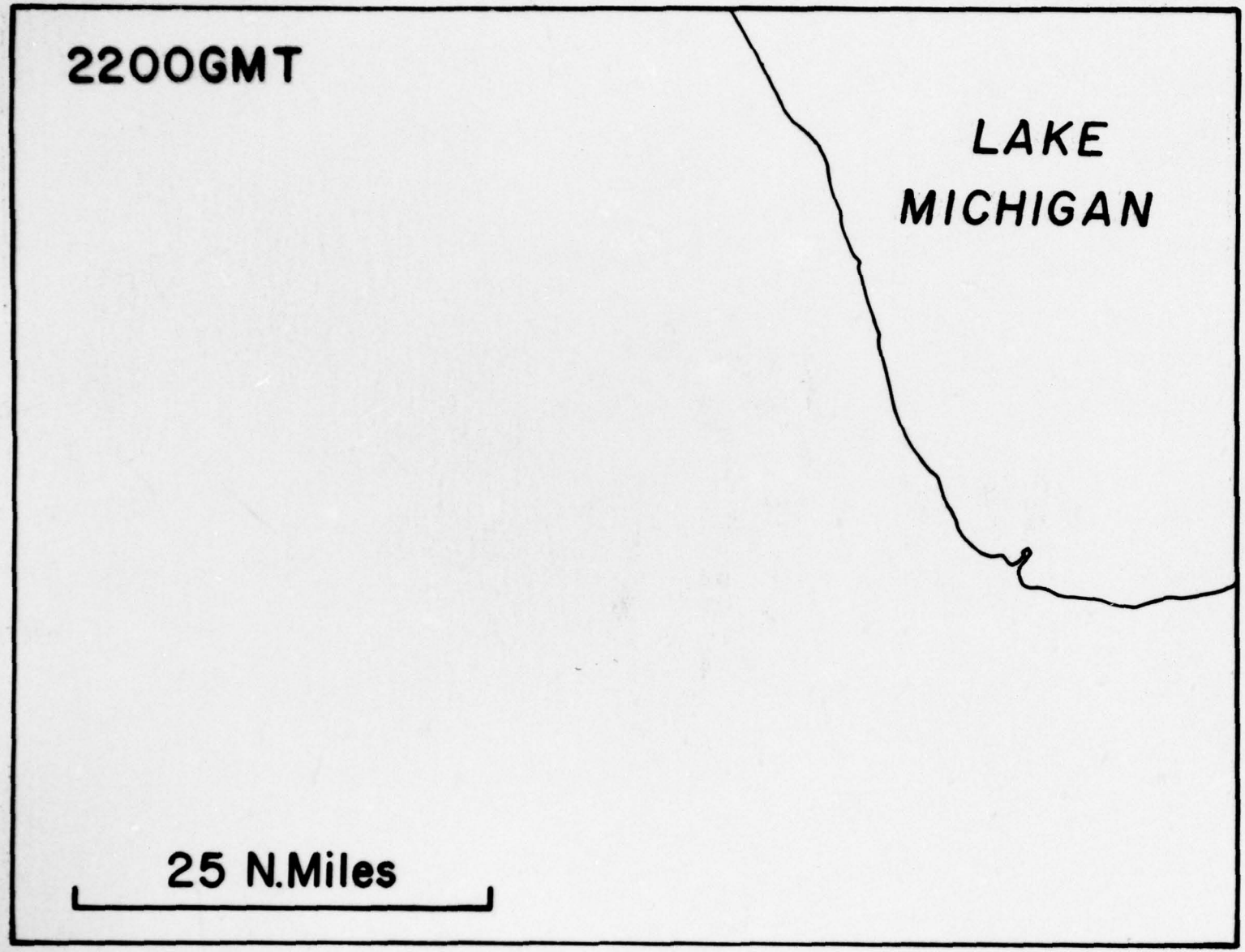

Bottom overlay for fig. 4

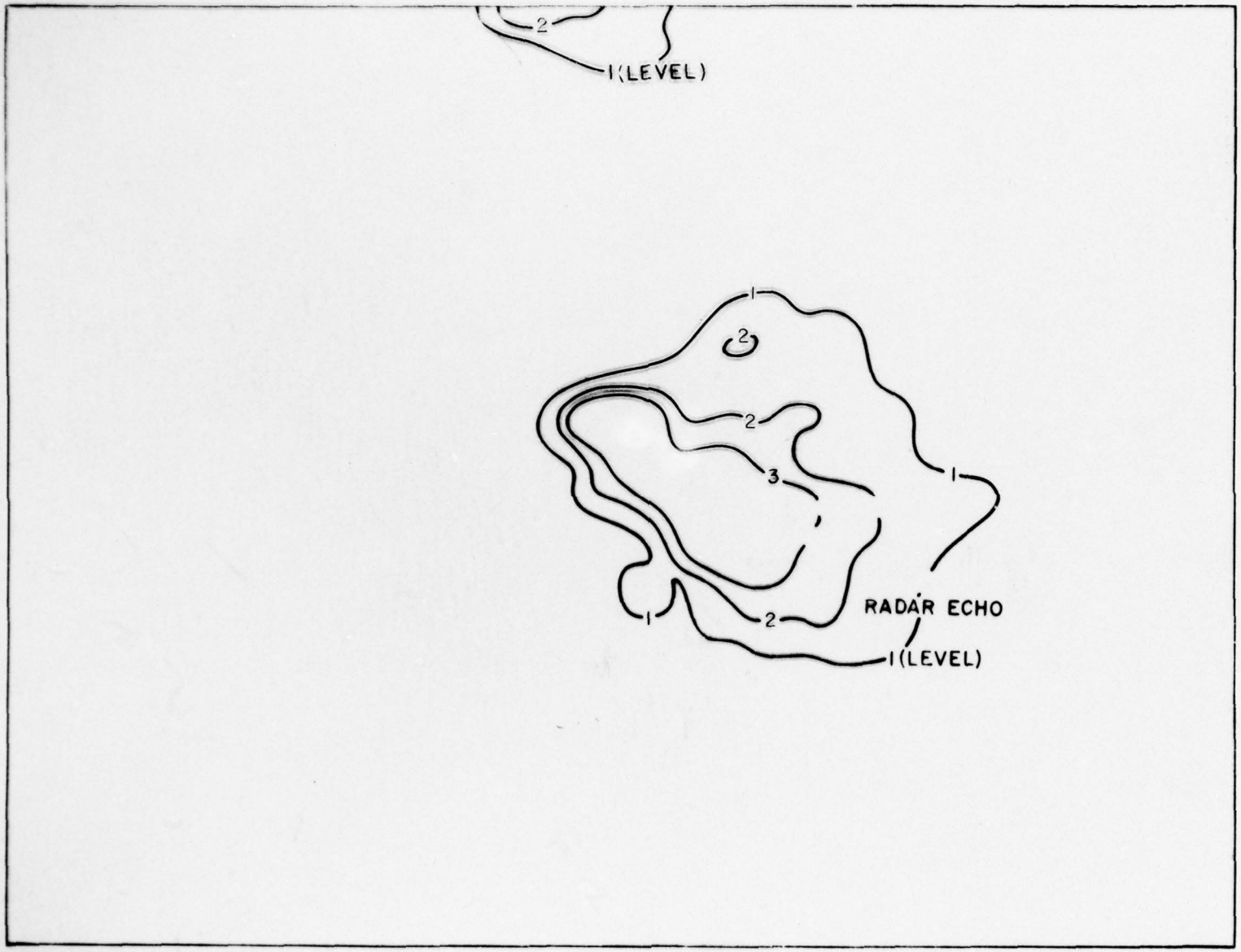

Top overlay for fig 5

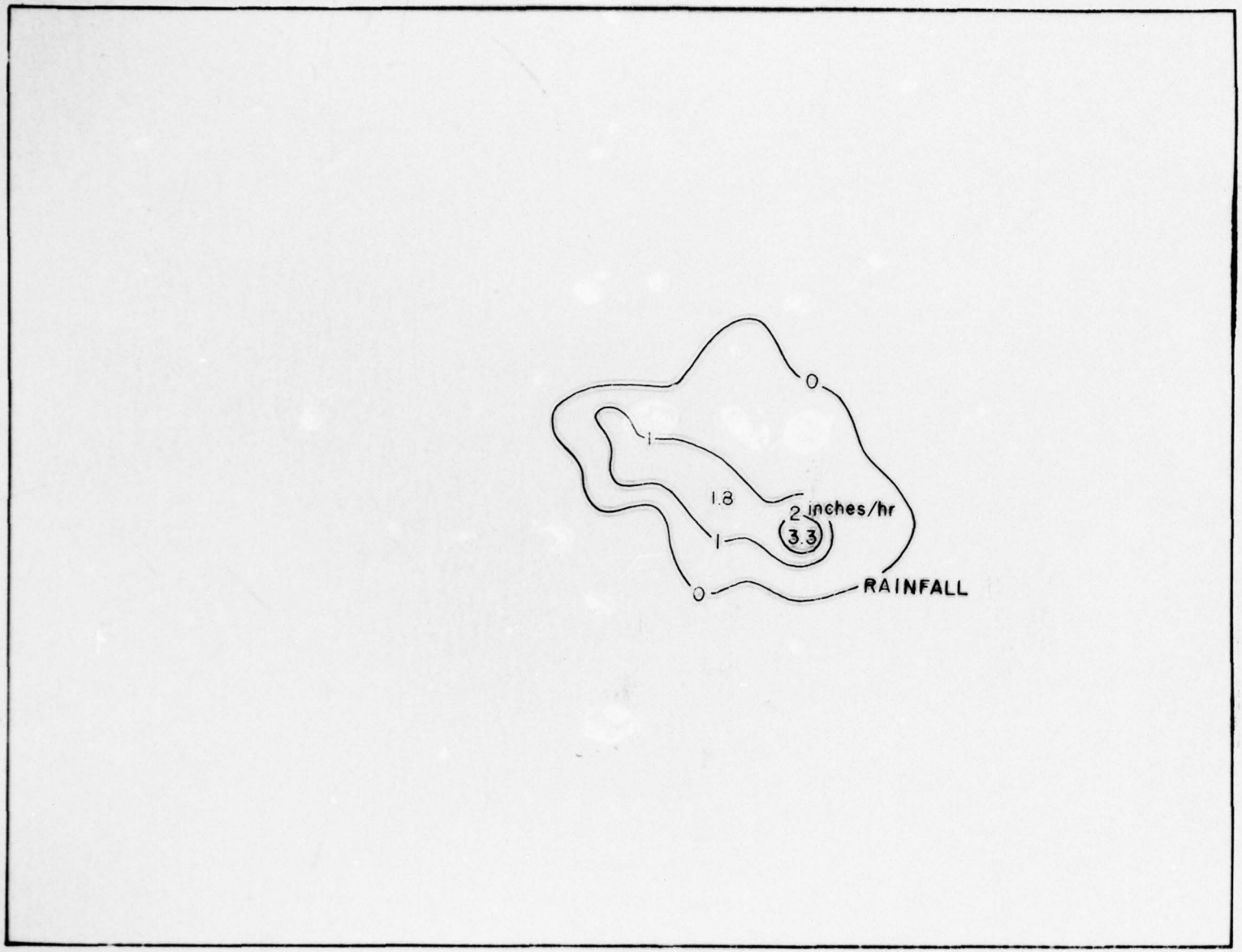

Second overlay for fig. 5

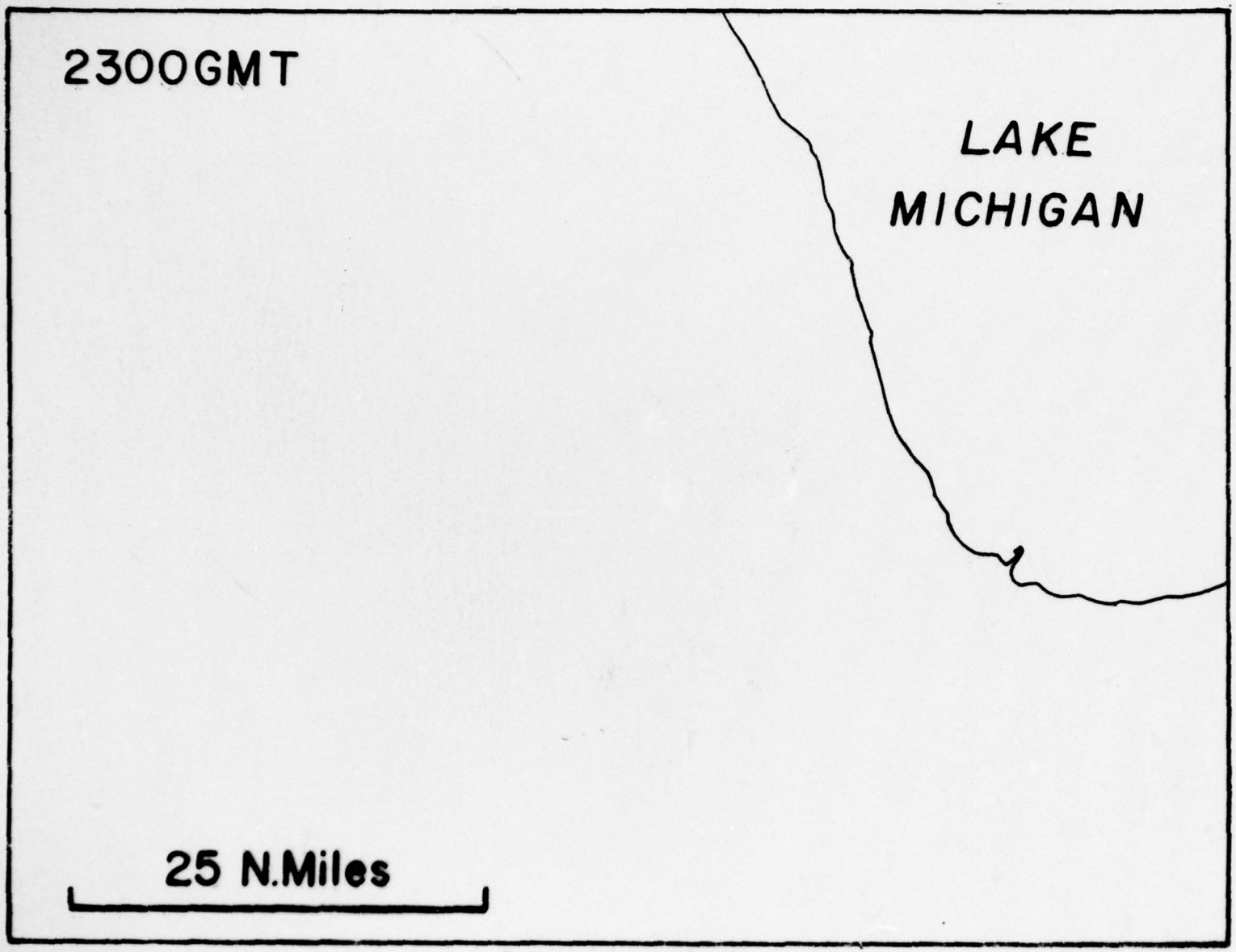

Bottom overlay for fig. 5

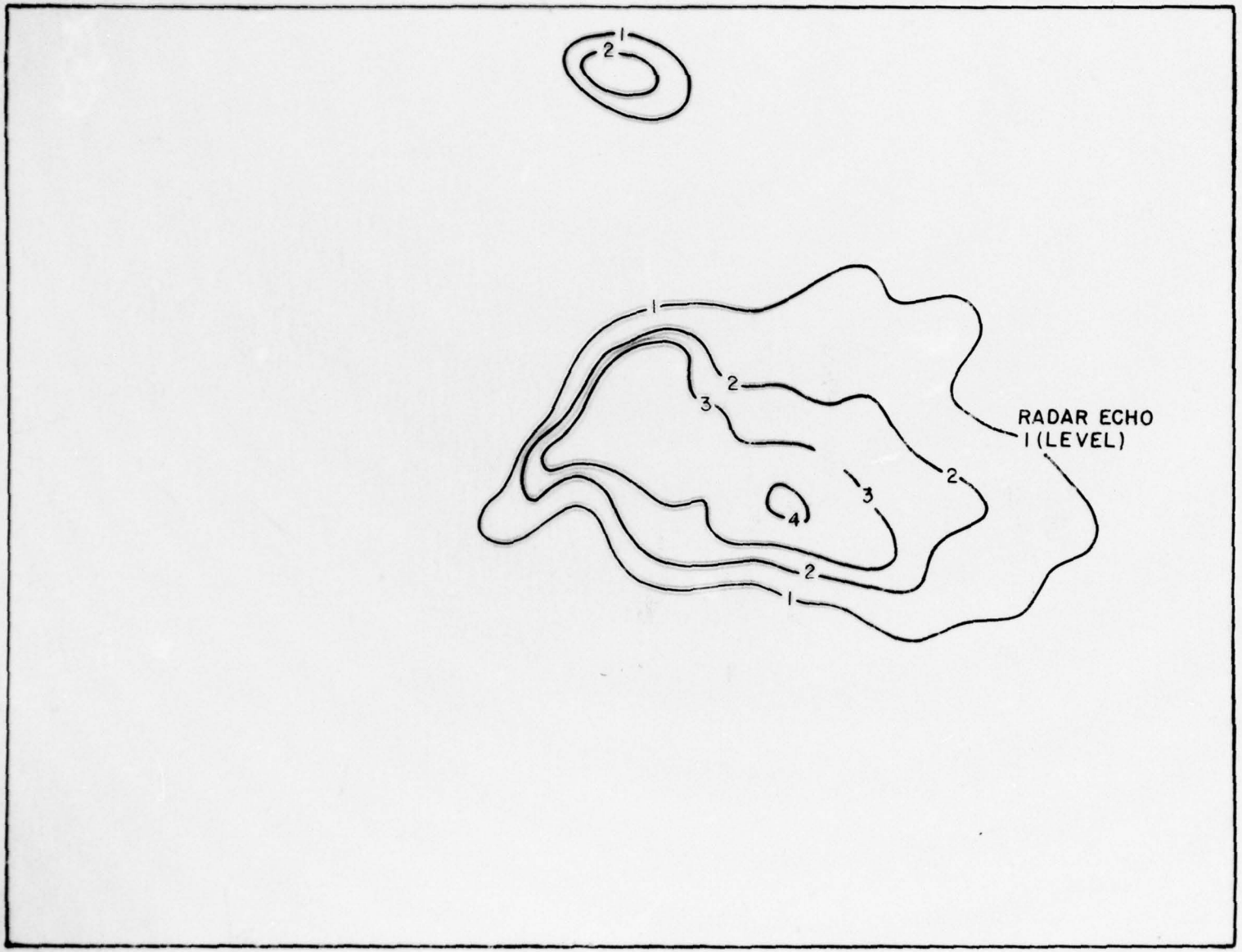

Top overlay for fig. 6

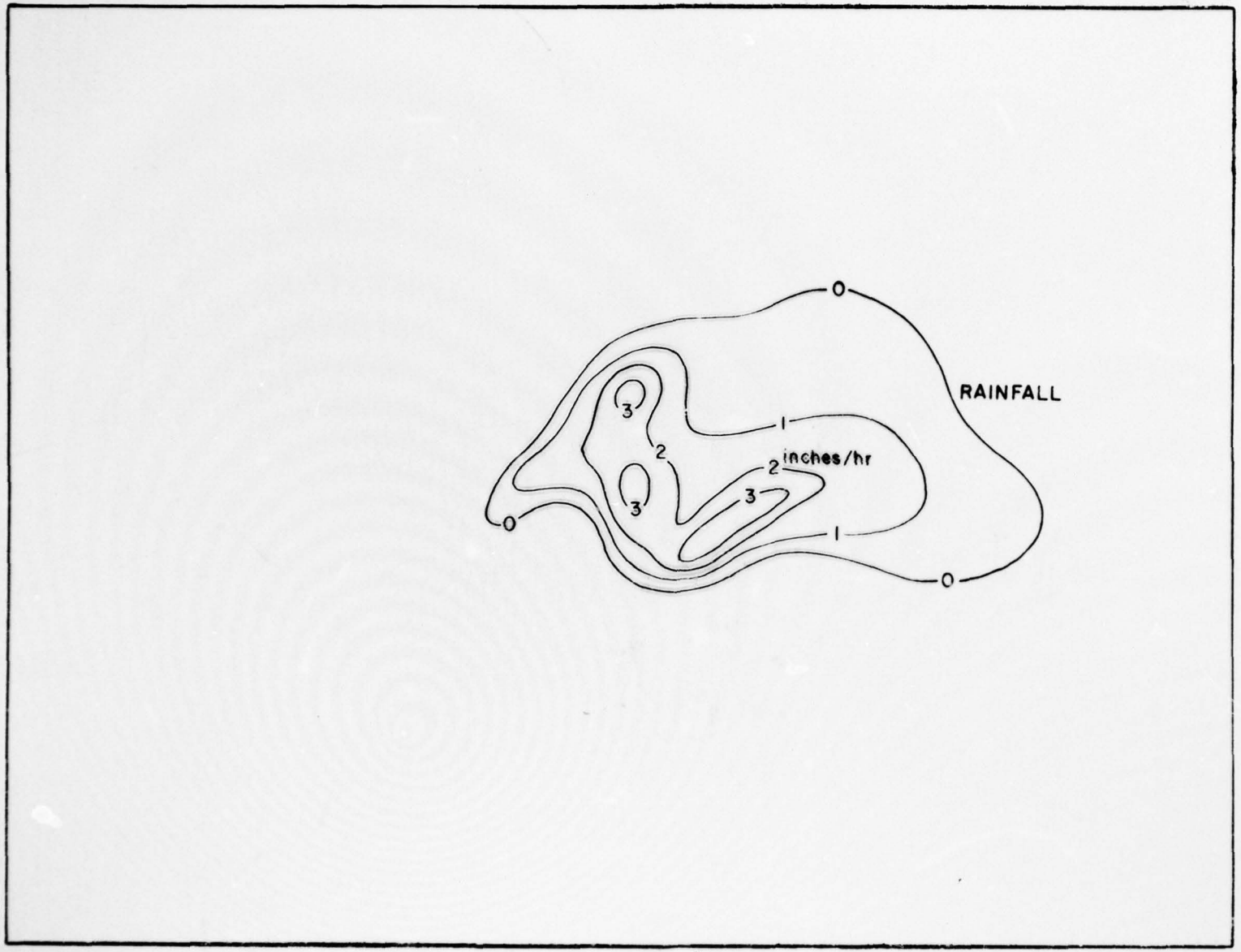

Second overlay for fig. 6

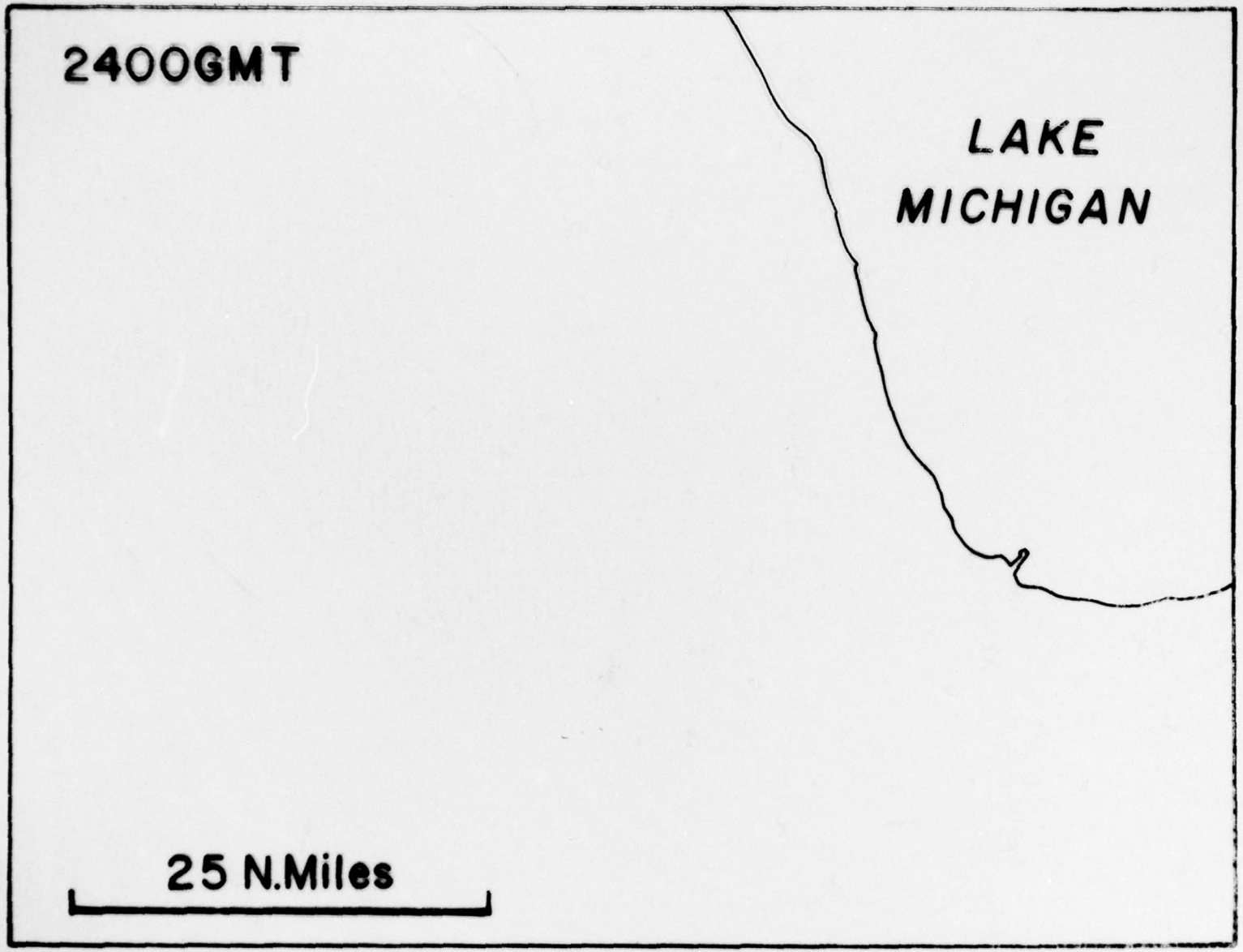

Bottom overlay for fig. 6